Review

CellPress

How cryo-EM is revolutionizing structural biology

Xiao-chen Bai, Greg McMullan, and Sjors H.W Scheres

MRC Laboratory of Molecular Biology, Francis Crick Avenue, Cambridge Biomedical Campus, Cambridge, CB2 0QH, UK

For many years, structure determination of biological macromolecules by cryo-electron microscopy (cryo-EM) was limited to large complexes or low-resolution models. With recent advances in electron detection and image processing, the resolution by cryo-EM is now beginning to rival X-ray crystallography. A new generation of electron detectors record images with unprecedented quality, while new image-processing tools correct for sample movements and classify images according to different structural states. Combined, these advances yield density maps with sufficient detail to deduce the atomic structure for a range of specimens. Here, we review the recent advances and illustrate the exciting new opportunities that they offer to structural biology research.

Historical context

Understanding how macromolecular complexes fulfill their complicated roles in the living cell is a central theme in molecular biology. Structural biology aims to deduce how such complexes function by determining the 3D arrangement of their atoms. Several techniques may be used to determine such structures. By far the most successful technique has been X-ray crystallography. Provided the complex of interest can be crystallized, this technique may yield atomic resolution and is not limited by the size of the complex. Nuclear magnetic resonance (NMR) may provide unique information about dynamics and interactions, but atomic structure determination is restricted to small complexes; that is, those with molecular weights (MWs) below 40–50 kDa. Both techniques typically require large amounts of relatively pure sample (on the order of several mg). Here, we review recent advances in cryo-EM imaging, which requires much less sample (0.1 mg may be enough), poses fewer restrictions on sample purity, and does not require crystallization.

EM of biological specimens has come a long way since the development of the first electron microscope, and the imaging of bacteriophages with it, by the Ruska brothers during the first half of the 20th century [1,2]. The main problem with looking at biological samples through an electron microscope is the degradation of the structural integrity of the sample. Given that electrons are scattered by air molecules, EM requires a high vacuum in the beam path, which compromises preservation of liquid aqueous samples. Even more importantly, biological macromolecules are susceptible to radiation damage through the breakage of chemical bonds by energy that is deposited in the sample by the electron beam.

Initial EM studies of biological samples used dehydrated samples or fixation techniques, many of which introduced artifacts in the structures. In particular, negative staining [3], where the water that surrounds the macromolecules is replaced by a dried solution of heavy-metal salt, became popular during the early 1960s and

Corresponding author: Scheres, S.H.W (scheres@mrc-lmb.cam.ac.uk).

Keywords: macromolecular complexes; single-particle analysis; cryo-electron microscopy; image processing; 3D reconstruction; electron detection; maximum-likelihood optimization.

0968-0004/

© 2014 Elsevier Ltd. All rights reserved. http://dx.doi.org/10.1016/j.tibs.2014.10.005

Glossary

3D reconstruction: the mathematical operation to calculate a 3D density map from a collection of 2D projection images.

Back-thinning: the process of making the supporting layer for the new detectors thinner.

Charge-coupled device (CCD): an older generation of digital cameras for cryo-EM was based on this technology. Given that the CCD chip is sensitive to photons, an extra layer on top of the chip is used to convert electrons into photons. This conversion is a major source of additional noise in cryo-EM images.

Counting mode: a mode of operation for the new detectors where individual incident electron events are quantized and counted to yield an image. This is the alternative to integrating mode.

Detective quantum efficiency (DQE): a measure for how much noise is added relative to the incoming signal due to errors in the detection process. A perfect detector does not add any noise and has a DQE of 1. In practice, all detectors add noise and have DQEs less than 1.

Direct electron detector: the latest generation of digital cameras for cryo-EM. 'Direct' refers to the fact that electrons are detected directly, in contrast to CCD cameras, where electrons are first converted into photons.

Integrating mode: a mode of operation for the new detectors where the recorded signals of all incident electron events are integrated to yield an image. This is the alternative to counting mode.

Monolithic active pixel sensor (MAPS): The direct electron detectors are based on this integrated circuit technology.

Movie mode: a mode of operation for the new detectors where multiple images are recorded during exposure of the sample to the electron beam.

Phase information: wave functions have an amplitude and a phase. In X-ray crystallography, measured intensities of reflections provide amplitude information, but the phase information needed to calculate the density map is lost. Cryo-EM images contain both amplitude and phase information, although both are hidden in large amounts of noise.

Resolution: a measure of the smallest detail that is discernible in a density map or image. Resolution is often measured in Å (1 Å =0.1 nm). Maps with better resolutions resolve smaller features. At resolutions better than 3.5 Å, many amino acid side-chains are resolved; at resolutions better than 4.8 Å, individual β strands are resolved; at resolutions better than 9 Å, α helices are resolved; and at worse resolutions only protein domains are resolved (Figure 1, main text).

Single-particle analysis: a cryo-EM procedure where individual macromolecular complexes that are frozen in a thin layer of vitreous ice are imaged. The 3D structure of the complex is reconstructed from projection images of individual complexes (called particles) in different relative orientations.

Vitreous ice: an amorphous form of solid water. The fact that this form of ice is not crystalline renders it particularly suitable for cryo-EM single-particle analysis.

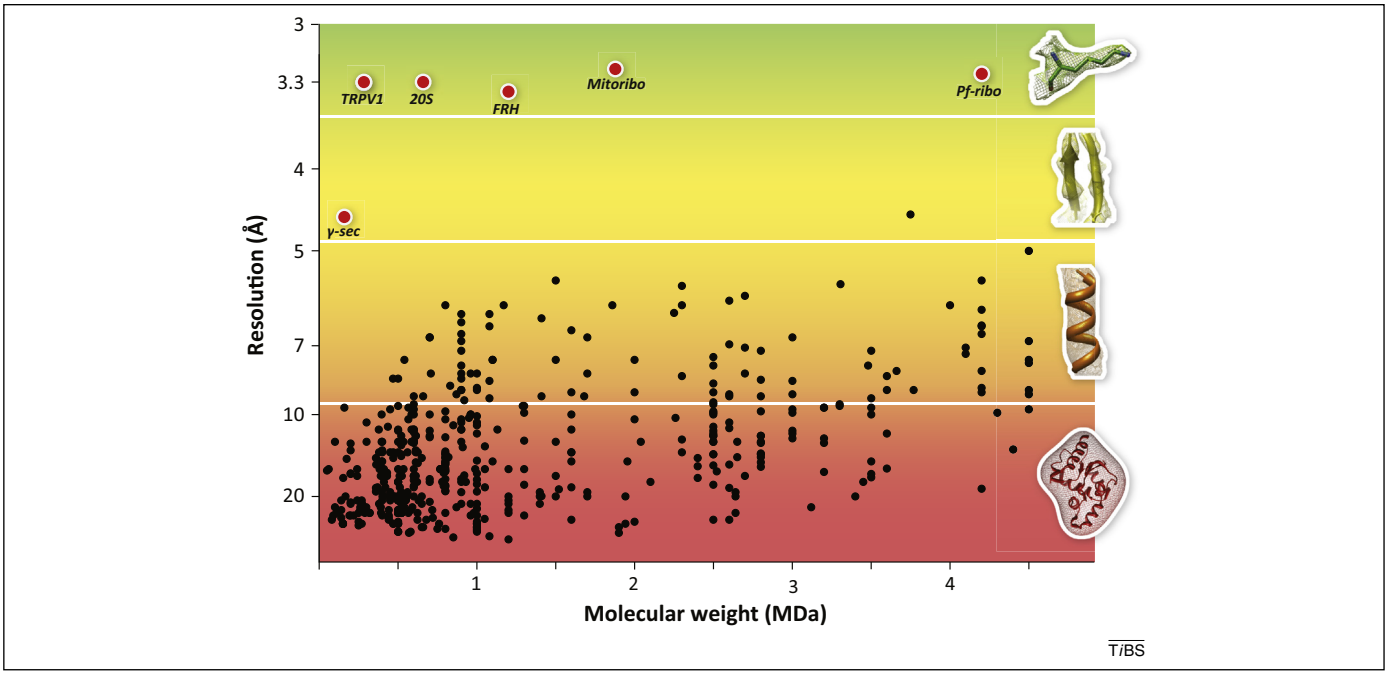

Figure 1. Revolutionary progress in cryo-electron microscopy (EM) single-particle analysis. The black dots represent single-particle cryo-EM structures that were released from the Electron Microscopy Data Bank (EMDB) between 2000 and 2012. The red dots are examples of recent progress in the field: γ-secretase (γ-sec), the transient receptor potential cation channel subfamily V member 1 (TRPV1), the 20S proteasome (20S), F420-reducing [NiFe] hydrogenase (FRH), the large subunit of the yeast mitochondrial ribosome (mitoribo), and the cytoplasmic ribosome of *Plasmodium falciparum* in complex with emetine (Pf-ribo). Whereas previously many structures only resolved protein domains (red area) or α helices (orange area), recent structures are detailed enough to distinguish β strands (yellow area) or even amino acid side-chains (green area).

remains so. Preserving the sample in a closer-to-native state was paramount to gaining a better understanding of biological function. Following early attempts by Henderson and Unwin [4,5] as well as Taylor and Glaeser [6,7], seminal work by Dubochet and coworkers showed how fully preserved samples could be imaged by freezing them in a thin layer of a noncrystalline form of solid water, called amorphous or vitreous ice (see Glossary) [8–10]. Given that vitreous ice is maintained at liquid nitrogen temperatures, this technique was termed 'cryo-EM'. Previously, DeRosier and Klug used negatively stained images of bacteriophage to show how 3D structures could be calculated from 2D projections of macromolecules in different directions. The combined application of cryo-EM imaging and 3D reconstruction to 2D crystals and helical arrays of proteins demonstrated its potential to obtain sufficient information to identify the positions of individual atoms [11–14].

The extensive symmetry in helical arrays and crystals greatly facilitates the 3D reconstruction process, but for many specimens such order is difficult to obtain. In the absence of long-range order, a purified solution of macromolecules may be imaged directly, and a 3D reconstruction may be calculated from projections of individual macromolecular complexes, or particles. The main limitation in this approach, called single-particle analysis, is that the particles are imaged in unknown relative orientations. High noise levels, especially at high resolution, which arise from using a limited electron dose to minimize radiation damage, complicate determining these orientations, particularly for smaller particles.

Early experimental assessment [15] and theoretical considerations [16] suggested that cryo-EM single-particle analysis could reach atomic resolution for macromolecular complexes as small as 100 kDa. For many years, this prospect seemed overly optimistic. Fastest progress was obtained for large icosahedral viruses. In 1997, single-particle reconstructions of the hepatitis B virus core particle resolved α helices for the first time [17,18]; in 2008, the amino acid backbone could be traced in cryo-EM maps of epsilon-15 virus, polyhedrosis virus, and the rotavirus inner capsid particle [19–21]; and in 2010, maps with sufficient details for *de novo* atomic model building were obtained for aquareovirus and adenovirus [22,23]. For particles without symmetry, 3D reconstruction is more difficult, and progress was much slower. Many of the early developments in image processing for asymmetric complexes were driven by work on negatively stained ribosomes during the 1980s [24,25]. Gradual progress in the development of these techniques and their adaptation for cryo-EM (e.g., [26–29], see [30] for an overview) led from ribosome cryo-EM structures with a resolution of around 40 Å during the early 1990s [31] to a resolution near 10 Å at the turn of the century [32]. Even more than a decade into the 21st century, only few cryo-EM structures of complexes with low or no symmetry have reached a resolution beyond 7–9 Å. At such resolution, α helices are visible as rod-like densities in the map, but β strands or amino acid side-chains are not resolved (Figure 1).

Since early 2013, progress in cryo-EM single-particle analysis has been so fast that is has been termed a revolution [33]. Figure 1 illustrates this progress: the black points represent structures deposited in the Electron Microscopy Data Bank (EMDB) between 2000 and 2012; the red points represent outcomes of the ongoing revolution. There are two important contributors to this rapid progress (Figure 2). The first, and probably most important factor, is the development of a new generation of electron detectors; the second is the development of improved image

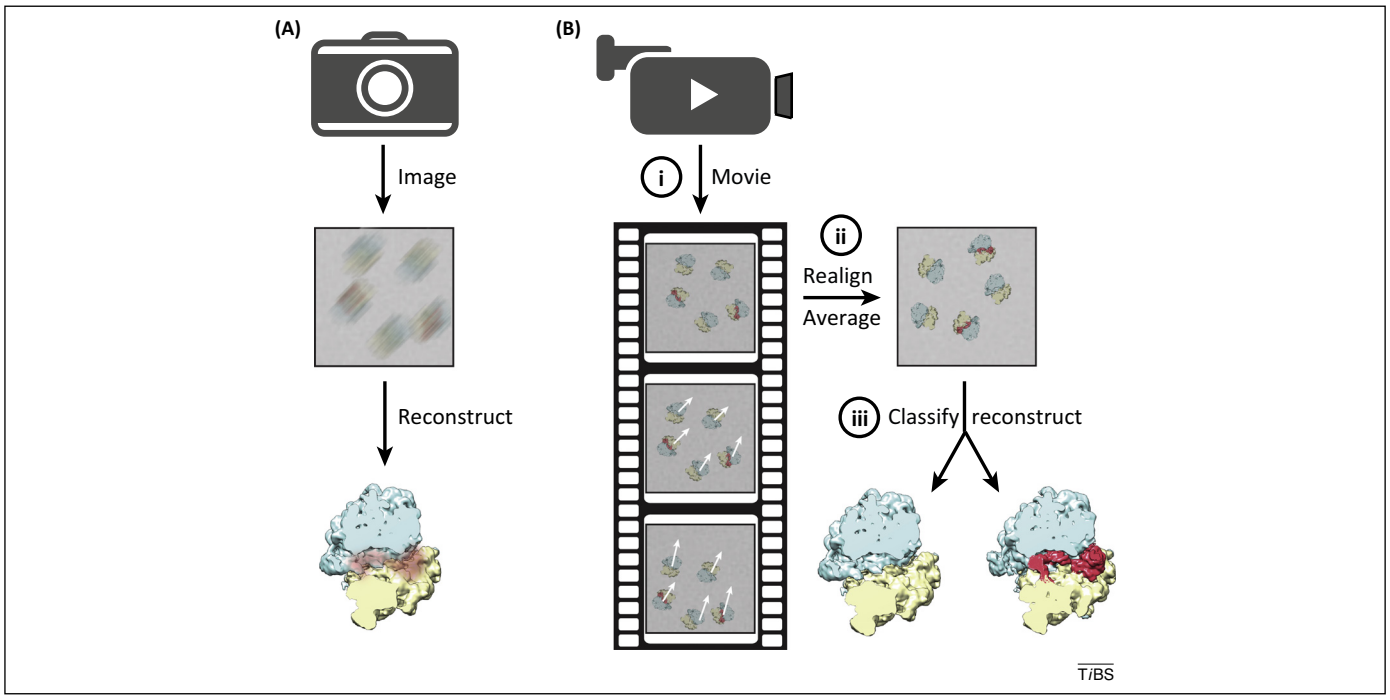

Figure 2. Recent technological advances. **(A)** Previously, noisier images were recorded on photographic film, beam-induced sample motion led to image blurring, and structurally different particles were often mixed in a single reconstruction. **(B)** Three recent advances yield better reconstructions: (i) digital direct-electron detectors yield data of unprecedented quality and allow recording movies during exposure; (ii) computer programs to realign the movie frames may correct for sample movements that are induced by the electron beam; and (iii) powerful classification methods lead to multiple structures from a sample mixture.

processing procedures. Here, we review both developments and describe the exciting, new opportunities that the latest cryo-EM technology has to offer structural biology research. Finally, we discuss outstanding problems of the technique that, if solved, would extend the scope of this technique even further.

What advances underlie the rapid progress?

Direct-electron detectors

Given that radiation damage strictly limits the number of electrons that can be used, cryo-EM images are intrinsically noisy and it is important to detect the available electrons as efficiently as possible. The detective quantum efficiency (DQE) of a detector expresses how the signal:-noise ratio of the incoming signal is degraded by errors in the detection process [34]. An ideal detector would not add any noise and so have a DQE of 1; however, in practice, all detectors add some noise and so have DQE values of less than 1. Figure 3 illustrates the effect of detector DQE in simulated cryo-EM images of a ribosome.

Until recently, photographic film remained the detector of choice for high-resolution cryo-EM, long after its use had faded out in other fields [35,36]. This was because of its unique combination of a large field-of-view and relatively high DQE of ~0.3. Alternatives, such as charge-coupled device (CCD) cameras [37–40], work well at low energies, but their DQE degrades to ~0.1 at the higher energies favored in cryo-EM. Still, the convenience of not having to develop and scan film, and the ability to integrate with automated data acquisition [41], have led to widespread use of CCD cameras [42,43].

Currently, the search for a convenient high-DQE detector (see [44] for a recent review) has converged on the use of monolithic active pixel sensors (MAPS) [45–47]. In these so-called 'direct electron detectors', incident electrons pass through a thin (~10-μm) semiconductor membrane where they deposit energy that is detected by electronics that are fabricated directly on the membrane. With these detectors, individual incident electrons can easily be seen. So too can electrons that initially pass through the membrane and are then backscattered from an underlying support matrix to pass though the membrane again. Given that the backscattered electrons lead to noise, the DQE is improved by removing as much of the support matrix as possible, in a process called 'back-thinning' [48]. The most recent detectors have a total thickness of less than 50 μm, which allows most electrons to pass straight through them without backscattering. Detectors of this type are now commercially available from three manufacturers: Direct Electron (DE), FEI (Falcon), and Gatan (K2).

The performance and characteristics of the currently available back-thinned direct electron detectors have been assessed in recent studies [49,50]. Each has a DQE above that of film, as well as the advantages of immediate feedback offered by an electronic detector. Given that even low-dose exposures may saturate these sensitive detectors, typical electron doses used in cryo-EM must be spread over multiple frames, and all available detectors now provide movie-mode functionality. The DE and Falcon detectors form an image by integrating the signal from the individual movie The limiting factor for the signal:noise ratio in the images of detectors that integrate signal, such as the DE and Falcon detectors, results from the fact that the incident electrons can deposit different amounts of energy and, hence, contributions to the output signal [51]. The K2 avoids this limitation by counting individual electron events rather than integrating the signal from these events [52–54]. To be practical, the counting mode requires

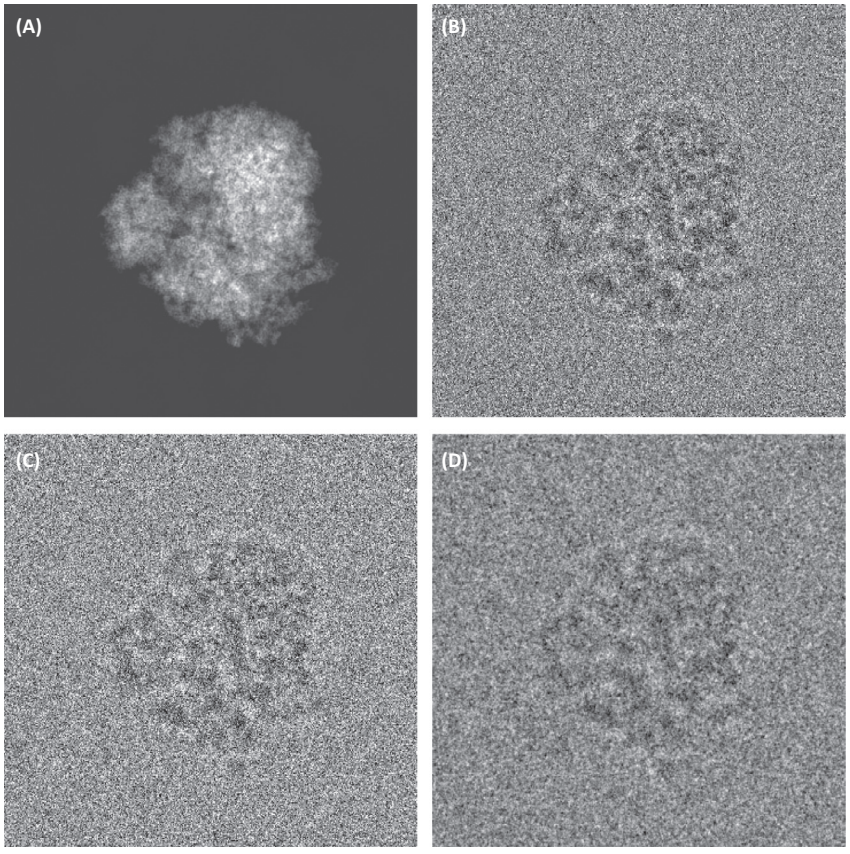

Figure 3. The effect of detector detective quantum efficiency (DQE) on cryo-electron microscopy (EM) images. **(A)** A perfect projection of a ribosome. **(B)** A simulation of the same image in cryo-EM with a perfect detector, that is, with a DQE of 1. The inversion of contrast and other artifacts arise from aberrations in the electron optics and the need to defocus to generate contrast. The high levels of noise arise from the finite number of electrons used: 20 electrons per $Å^2$ in this simulation. **(C)** The same simulated cryo-EM image, but with a DQE representative of the new detectors. **(D)** The same image, but with a DQE representative of a CCD camera.

recording movies at a high frame rate (at least 400 frames per second), and dedicated hardware is needed to produce an image in real time. Moreover, the counting mode requires long exposures times that may become problematic when the experimental support is not stable. Still, counting offers large benefits to the lower resolution information in output images, which is crucial for the orientation determination of the individual particles. However, the difficulties in determining where an electron hit the detector mean that an integrating detector, such as the back-thinned Falcon, is still better for obtaining high-resolution information [50].

Improved image processing

Two developments in image processing have synergized with the new detectors to obtain better reconstructions. The first development addresses the difficulties in dealing with structurally heterogeneous samples; the second addresses the problem of the irradiating electron beam itself inducing movement of the sample. If left untreated, both issues will result in a severe loss of information.

Most samples of macromolecular complexes contain more than one unique 3D structure due to compositional or conformational heterogeneity. If projections of different structures are not classified into structurally homogeneous subsets, their combination into a single 3D reconstruction will result in a blurry map at best. The classification problem is complicated because it is often hard to distinguish between projections from different directions and projections of different 3D structures. Early so-called 'supervised' 3D classification attempts relied heavily on prior knowledge of the structural variability in the sample [55,56], which is not generally available. The breakthrough that allowed generally applicable unsupervised 3D classification came from the development of statistical algorithms that were based on maximum-likelihood procedures [57,58]. Subsequently introduced alternatives were based on multivariate statistical analysis [59], 3D variance calculation by bootstrapping [60], nonstatistical multiparticle refinement [61], and partial implementations of the maximum-likelihood approach [62]. With the introduction of an (empirical) Bayesian approach to single-particle analysis, a statistical framework was established where optimal parameters to reduce noise in the reconstructions are inferred from the data without expert-user intervention [63]. Implementation of this regularized likelihood approach in the RELION program [64] has proven to be a powerful tool for both 3D classification and high-resolution reconstruction that has quickly gained popularity (Table 1).

The second development in image processing is closely related to the development of the new detectors. As soon as the electron beam hits the thin film of vitreous ice, chemical bonds in the sample are broken and charges start to build up. Although ultimately this destroys the entire

Table 1. Cryo-EM single-particle reconstructions that have been determined on a direct-electron detector to a resolution better than 5 Å (as of June 2014)

Sample	EMDB entry	Release date	MW (MDa)	Point group	Detector	3D classification?	Beam-induced motion correction?	Software	Resolution (Å)	Refs
80S ribosome + emetine[a]	2660	Jun 2014	4.2	C1	Falcon	Yes	Yes	RELION [64]	3.2	[76]
Yeast mitoribosome (LSU)[a]	2566	Apr 2014	1.9	C1	Falcon	Yes	Yes	RELION	3.2	[71]
TRPV1[a]	5778	Dec 2013	0.3	C4	K2	Yes	Yes	RELION	3.3	[69]
20S proteasome[a]	5623	May 2013	0.7	D7	K2	No	Yes	FREALIGN [87]	3.3	[53]
FRH[a]	2513	Feb 2014	1.2	T	Falcon	No	Yes	RELION	3.4	[70]
80S ribosome + CrPV-IRES	2599	May 2014	3.2	C1	Falcon	Yes	Yes	RELION	3.6	[81]
TRPV1 + DkTx + RTX	5776	Dec 2013	0.3	C4	K2	Yes	Yes	RELION	3.8	[68]
Dengue virus	2485	Nov 2013	50	I	Falcon	No	No	EMAN [88], MPSA [89]	4.1	[90]
80S ribosome + eIF5B	2421	Nov 2013	4.2	C1	Falcon	Yes	Yes	RELION	4.3	[79]
Rotavirus	5488	Sep 2012	35	I	DE	No	Yes	FREALIGN	4.4	[66]
γ-secretase[a]	2678	Jun 2014	0.17	C1	K2	Yes	Yes	RELION	4.5	[77]
80S ribosome	2275	Jan 2013	4.2	C1	Falcon	Yes	Yes	RELION	4.5	[67]
Sulfolobus turreted virus	5584	May 2013	75	I	Falcon	No	No	FREALIGN	4.5	[91]
Mammalian mitoribosome (LSU)	2490	Dec 2013	1.6	C1	Falcon	No	No	SPIDER, IMAGIC [92], RELION	4.9	[93]

[a]Shown as red points in Figure 1 (main text).

sample, even early on in the exposure the forces involved will induce motion within the sample, which leads to blurring of the recorded images on conventional CCDs or photographic film (Figure 2). Using a prototype of a DE detector, Niko Grigorieff and colleagues were the first to exploit the movie mode of the new detectors to characterize beam-induced sample movements. They observed doming of the ice layer, and showed that realignment of the individual movie frames could correct for these movements, thereby improving the signal:noise ratios of individual particle images [65,66].

Soon thereafter, the first major improvements in resolution of reconstructed maps were obtained in independent projects at the University of California in San Francisco (UCSF) and the Medical Research Council (MRC) in Cambridge, UK. At UCSF, 20S proteasome particles were imaged on the K2 detector in counting mode, and an algorithm for beam-induced motion correction of large fields of view was proposed [53,54]. Using 120 000 particles (with 14-fold symmetry), a map at 3.2 Å resolution was obtained in which almost all amino-acid side-chains were clearly resolved. Simultaneously, at the MRC, ribosomes were imaged on a back-thinned Falcon detector, and a motion-correction algorithm was developed that tracked motions of individual particles inside the Bayesian framework [67]. Using only 35 000 (asymmetric) particles, 4 Å details, such as side-chain densities for large amino acids, were observed. These two structures provided the first glimpse of the vastly increased potential for cryo-EM structure determination using the new detectors in combination with beam-induced motion correction.

For many in the field, these first results came as a surprise, probably because the synergy between the new detectors and the improved image processing algorithms was unexpected. On the one hand, images with stronger signals directly led to higher resolution maps. On the other hand, the less noisy images allowed the new image-processing algorithms to perform better than before. This led to more homogeneous data sets with less motion-induced blurring, so that the orientation of each particle could be determined more accurately. The combined effect on the final resolution of the reconstructed maps was stronger than many had expected.

What is now possible?

Table 1 summarizes all cryo-EM structures that were determined using the new detectors to a resolution better than 5 Å that had been released from the EMDB by June 2014. Here, we use a few examples of these structures to illustrate the new opportunities for structural biology research that these advances provide.

Solving structures de novo

Previously, the interpretation of low-resolution cryo-EM maps often relied on fitting atomic models from X-ray crystallography or NMR. Three groups that had early access to (prototypes of) the new detectors produced the first *de novo* atomic models by cryo-EM that exploited the advances outline above. Using the K2 detector, the Cheng group at UCSF solved the structure of the transient receptor potential cation channel subfamily V member 1 (TRPV1) channel [68,69]; using the Falcon detector, the Vonck group at the Max Planck Institute for Biophysics in Frankfurt solved the structure of F420-reducing [NiFe] hydrogenase (FRH) [70]; and at the MRC, the structure of the large subunit of the mitochondrial ribosome from yeast was solved [71]. In all three cases, resolutions beyond 3.5 Å were obtained, at which most of the amino acid side-chains are clearly visible, and near-complete atomic models could be built *de novo* (Figure 4A–C).

At these resolutions, cryo-EM density maps are reminiscent of those obtained by X-ray crystallography. Therefore, it is not surprising that tools developed for the building and stereochemical refinement of crystal

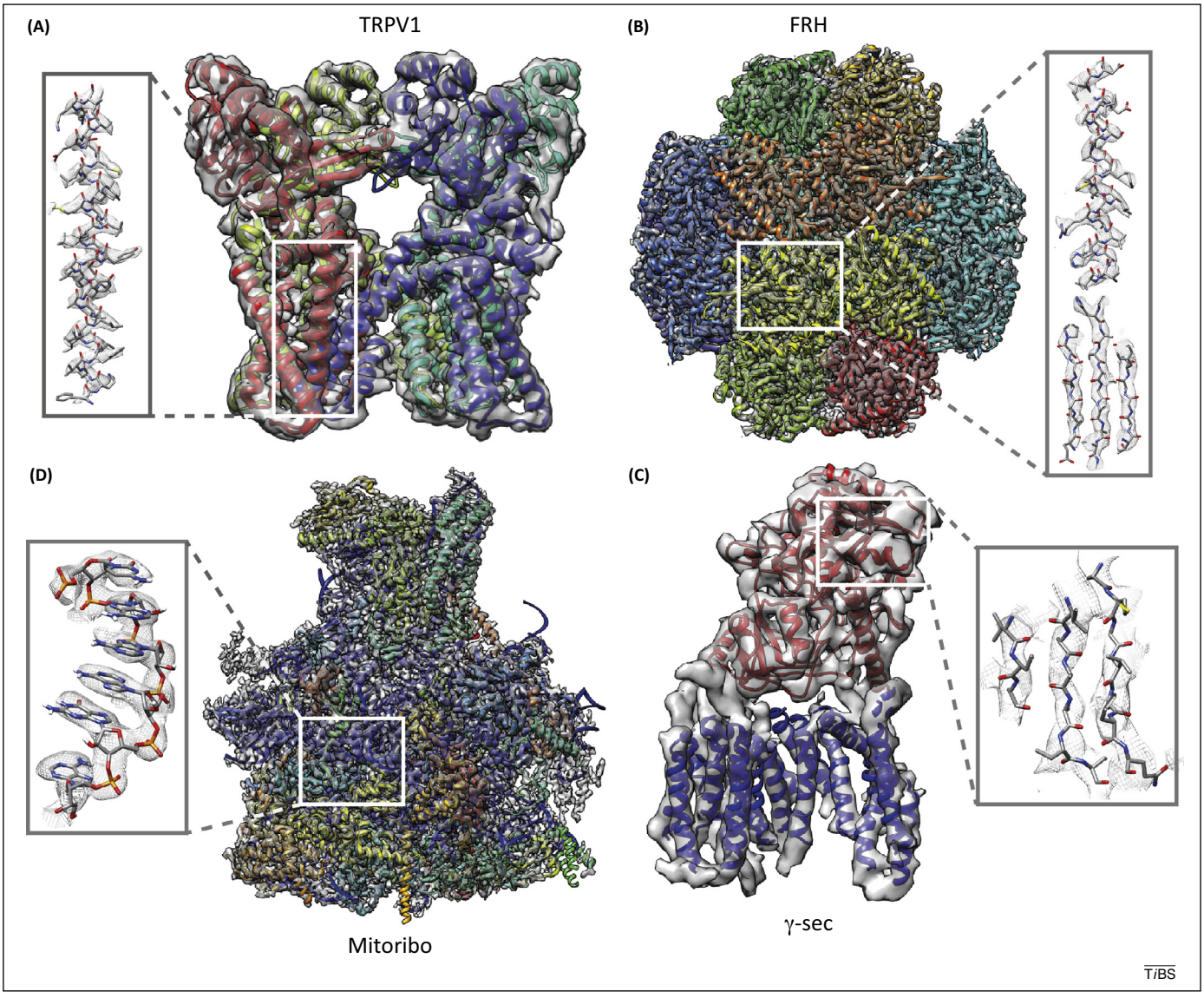

Figure 4. High-resolution cryo-electron microscopy (EM) maps with *de novo*-built atomic models. Atomic models and cryo-EM density maps are shown for the transient receptor potential cation channel subfamily V member 1 (TRPV1) ion channel **(A)**, F420-reducing [NiFe] hydrogenase **(B)**, large subunit of the yeast mitochondrial ribosome **(C)**, and γ-secretase **(D)**. The resolution of the first three structures is close to 3 Å, and density for many side chains and individual RNA bases is visible in these maps; the resolution of the γ-secretase structure is 4.5 Å, at which bulky side chains are visible and β strands are well resolved (insets).

structures could be readily adopted for cryo-EM. The main difference is that the phase information of the X-ray reflections is lost in the diffraction experiment, whereas this information is preserved in cryo-EM images. This is likely also the reason that cryo-EM maps are clearer and, thus, resolve more detail than do X-ray maps at the same nominal resolution. The models for all three structures mentioned above were built using the graphics program COOT [72], but only the mitochondrial ribosome structure was also refined, in this case using the program REFMAC [73]. Both programs were developed for, and are widely used in, X-ray crystallography. Combined with new cryo-EM-specific tools to monitor overfitting [71,74,75], geometrically correct atomic models may now be obtained *de novo* from cryo-EM reconstructions.

Visualizing small-molecule compounds

Another outcome of near-3 Å resolution is that small-molecule compounds, such as co-factors or inhibitors, may now be identified in cryo-EM maps. Along with an empty TRPV1 structure, the UCSF team also solved this structure in complex with a peptide toxin called double-knot toxin (DkTx) and the vanilloid agonist resiniferatoxin (RTX) [68]. Although at a resolution of 3.8 Å the exact orientation of the small agonist could not be determined, its location and residues involved in binding could be identified from the cryo-EM reconstruction (Figure 5A).

Later in 2013, the structure of the cytoplasmic ribosome of *Plasmodium falciparum* in complex with the antiprotozoan drug emetine was solved at a resolution of 3.2 Å. In this case, both the position and orientation of the drug could be determined unambiguously (Figure 5B), thereby providing detailed molecular insights into the mode of action of this general eukaryotic translation inhibitor [76].

Towards solving smaller complexes

Now that near-atomic resolution has been consolidated for a range of specimens, the question arises as to where the

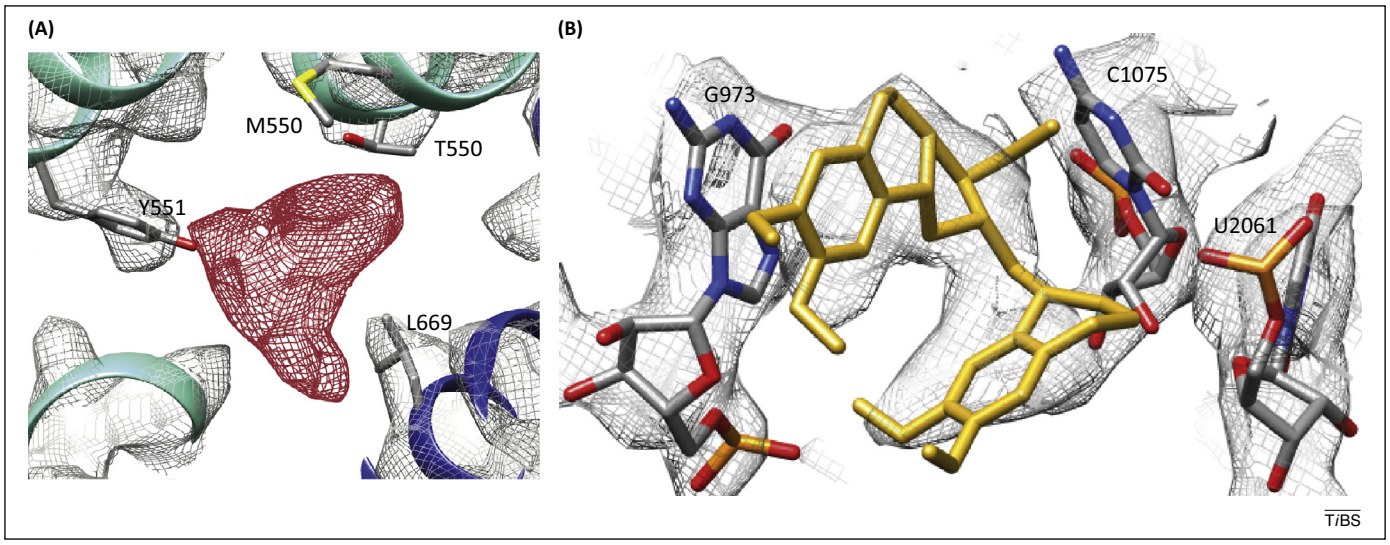

Figure 5. Visualization of small-molecule compounds. **(A)** A reconstruction of the transient receptor potential cation channel subfamily V member 1 (TRPV1) ion channel in complex with the vanilloid agonist resiniferatoxin (RTX) at 3.8 Å resolution unambiguously identifies the location of the agonist (red) and the protein residues that interact with it. At this resolution, the exact orientation of the agonist remains unknown. **(B)** At 3.2 Å resolution, a reconstruction of the cytoplasmic ribosome of *Plasmodium falciparum* in complex with the antiprotozoan drug emetine (yellow) reveals the nature of the chemical interactions between the drug and its binding pocket.

new size limits lie. Both the ribosome and FRH might be considered easy targets for cryo-EM because they are relatively large, and the latter also has tetrahedral symmetry. The minimal TRPV1 channel is smaller (0.3 MDa) and thereby more challenging, although also in this case fourfold symmetry expedites 3D reconstruction. Currently, the smallest complex subjected to the new methodology is γ-secretase [77]. This asymmetric membrane complex comprises four different proteins with a total molecular weight of 170 kDa (plus an additional ~60kDa of unordered oligosaccharides). Imaging on a K2 detector in counting mode and performing reconstruction with a modified motion correction algorithm [78] led to a 4.5 Å map (Figure 4D), which proved insufficient for *de novo* model building. In this case, a partially complete model for the extracellular domain could be proposed based on a homologous structure, but transmembrane helices were modeled as polyalanines only and their assignment to the four different proteins remained elusive.

Working with heterogeneous samples

Given that crystallization is often hampered by structural heterogeneity within a sample, classification of structurally heterogeneous cryo-EM data sets is a major asset for the structural biologist, particularly when only small amounts are available or further biochemical purification is difficult. Of the structures in Table 1, the 80S ribosome in complex with eIF5B [79] is perhaps the most extreme example. In this case, because of incomplete factor binding, nonspecific tRNA hydrolysis and ribosomal subunit disintegration, the structural state of interest represented approximately 3% of the recorded particle images. Still, unsupervised maximum likelihood classification could identify these particles, and a 6.6 Å map could be calculated from only 5000 particles.

Three other examples are the mitochondrial large ribosomal subunit from yeast [71] and the 80S ribosome bound to either the Taura syndrome virus (TSV) internal ribosome entry site (IRES) [80], or the cricket paralysis virus (CrPV) IRES [81]. In the former, mitochondrial ribosome preparations were contaminated with cytoplasmic ribosomes that stuck to the outside of extracted mitochondrial membranes. In the latter two, different rotational states between the large and the small subunit were present in the sample. In all three cases, maximum likelihood-based 3D classification procedures were able to separate particles corresponding to the different structures.

However, there are important limitations on what can be achieved with the current 3D classification algorithms. All four examples just discussed concern ribosomes. For complexes that are smaller than ribosomes, or that contain continuously flexing domains, separation of the particles in structurally homogeneous subsets is difficult. For example, in the case of γ-secretase, 3D classification served to enrich the data set with good particles, but density for one third of the extracellular domain was too poor to model, and density for many flexible loops and all sugars was missing. Therefore, with the currently available classification algorithms, unresolved structural heterogeneity remains an important hurdle in reaching near-atomic resolution for a range of specimens.

Where do we go from here?

The advances described here will cause an avalanche of high-resolution cryo-EM structures in the coming years. In particular for large and rigid complexes, and those with some form of symmetry, many projects will reach a resolution that allows *de novo* building of atomic models. Moreover, determining the structures of these complexes locked in different functional states by small-molecule compounds will contribute to better understanding of how they work. For many such projects, biochemical sample preparation will become the main bottleneck, while solving the actual cryo-EM structure will be easier and take less time. However, for smaller (<200–300 kDa), unstable or flexible complexes, obtaining near-atomic resolution maps may still be difficult and time consuming. For many such projects, resolving α-helices as rod-like densities may well represent the best that one can still do.

Box 1. Outstanding questions

- How can we develop an electron detector with a DQE that approaches 1?
- How can we stop beam-induced motion?
- How can we improve algorithms for flexible specimens?
- How can we improve user-friendliness and throughput, while decreasing the cost of the technique?

Nevertheless, there is room for significant further advances in the technology (Box 1). First, the technological limits of making better CMOS detectors have not yet been reached. Whereas average DQEs are currently ~0.5, values of ~0.8 should ultimately be possible with a detector in counting mode. Making even thinner detectors will help, as well as faster read-outs and better counting algorithms to detect the position of incident electrons. Second, although motion-correction algorithms have been useful in improving resolution thus far, stopping beam-induced motion would be even better. Early radiation damage experiments showed that 99% of the 3 Å information in catalase crystals is destroyed after an almost ten times lower dose than typically used in single-particle analysis [82]. Yet, during these initial stages of irradiation the beam-induced motion is too fast to efficiently correct for [53,78]. Therefore, stopping the sample from moving altogether would yield a drastic improvement in the preservation of high-resolution information. Ongoing research to accomplish this comprises alternative designs of the experimental support [83–85] and novel data collection methods [86]. Third, there is a clear need for even better image classification methods to deal with the range of biological samples that display large amounts of structural heterogeneity. Finally, the field would benefit greatly from improved accessibility of the technique. Although progress has been made in high-throughput and automation [41], electron microscopists are typically still expert scientists, and the elevated costs of purchasing and maintaining modern microscopes makes experimental time both scarce and expensive. Further improvements seem likely if both academia and industry continue their efforts to address these issues, and cryo-EM is likely to continue to push the boundaries of structural biology in the coming years.

References

1 Ruska, H. (1941) Über ein neues bei der bakteriophagen Lyse auftretendes Formelement. *Naturwissenschaften* 29, 367–368
2 Ruska, H. *et al.* (1939) Die Bedeutung der Übermikroskopie für die Virusforschung. *Arch. Für Gesamte Virusforsch.* 1, 155–169
3 Brenner, S. and Horne, R.W. (1959) A negative staining method for high resolution electron microscopy of viruses. *Biochim. Biophys. Acta* 34, 103–110
4 Henderson, R. and Unwin, P.N. (1975) Three-dimensional model of purple membrane obtained by electron microscopy. *Nature* 257, 28–32
5 Unwin, P.N. and Henderson, R. (1975) Molecular structure determination by electron microscopy of unstained crystalline specimens. *J. Mol. Biol.* 94, 425–440
6 Taylor, K.A. and Glaeser, R.M. (1974) Electron diffraction of frozen, hydrated protein crystals. *Science* 186, 1036–1037
7 Hayward, S.B. and Glaeser, R.M. (1979) Radiation damage of purple membrane at low temperature. *Ultramicroscopy* 4, 201–210
8 Adrian, M. *et al.* (1984) Cryo-electron microscopy of viruses. *Nature* 308, 32–36
9 Dubochet, J. *et al.* (1981) Low temperature electron microscopy. *Annu. Rev. Biophys. Bioeng.* 10, 133–149
10 Dubochet, J. *et al.* (1988) Cryo-electron microscopy of vitrified specimens. *Q. Rev. Biophys.* 21, 129–228
11 Nogales, E. *et al.* (1998) Structure of the alpha beta tubulin dimer by electron crystallography. *Nature* 391, 199–203
12 Kühlbrandt, W. *et al.* (1994) Atomic model of plant light-harvesting complex by electron crystallography. *Nature* 367, 614–621
13 Gonen, T. *et al.* (2005) Lipid-protein interactions in double-layered two-dimensional AQP0 crystals. *Nature* 438, 633–638
14 Unwin, N. (2005) Refined structure of the nicotinic acetylcholine receptor at 4A resolution. *J. Mol. Biol.* 346, 967–989
15 Zhou, Z.H. and Chiu, W. (1993) Prospects for using an IVEM with a FEG for imaging macromolecules towards atomic resolution. *Ultramicroscopy* 49, 407–416
16 Henderson, R. (1995) The potential and limitations of neutrons, electrons and X-rays for atomic resolution microscopy of unstained biological molecules. *Q. Rev. Biophys.* 28, 171–193
17 Böttcher, B. *et al.* (1997) Determination of the fold of the core protein of hepatitis B virus by electron cryomicroscopy. *Nature* 386, 88–91
18 Conway, J.F. *et al.* (1997) Visualization of a 4-helix bundle in the hepatitis B virus capsid by cryo-electron microscopy. *Nature* 386, 91–94
19 Jiang, W. *et al.* (2008) Backbone structure of the infectious epsilon15 virus capsid revealed by electron cryomicroscopy. *Nature* 451, 1130–1134
20 Yu, X. *et al.* (2008) 3.88 A structure of cytoplasmic polyhedrosis virus by cryo-electron microscopy. *Nature* 453, 415–419
21 Zhang, X. *et al.* (2008) Near-atomic resolution using electron cryomicroscopy and single-particle reconstruction. *Proc. Natl. Acad. Sci. U.S.A.* 105, 1867–1872
22 Zhang, X. *et al.* (2010) 3.3 Å cryo-EM structure of a nonenveloped virus reveals a priming mechanism for cell entry. *Cell* 141, 472–482
23 Liu, H. *et al.* (2010) Atomic structure of human adenovirus by cryo-EM reveals interactions among protein networks. *Science* 329, 1038–1043
24 Verschoor, A. *et al.* (1984) Three-dimensional reconstruction of the 30 S ribosomal subunit from randomly oriented particles. *J. Mol. Biol.* 178, 677–695
25 Radermacher, M. *et al.* (1987) Three-dimensional structure of the large ribosomal subunit from *Escherichia coli*. *EMBO J.* 6, 1107–1114
26 Frank, J. *et al.* (1981) Computer averaging of electron micrographs of 40S ribosomal subunits. *Science* 214, 1353–1355
27 Van Heel, M. and Frank, J. (1981) Use of multivariate statistics in analysing the images of biological macromolecules. *Ultramicroscopy* 6, 187–194
28 Harauz, G. and van Heel, M. (1986) Exact filters for general geometry three dimensional reconstruction. *Optik* 73, 146–156
29 Frank, J. and van Heel, M. (1987) On the correction of the contrast transfer function in biological electron microscopy. *Optik* 98, 125–129
30 Frank, J. (2006) *Three-dimensional Electron Microscopy of Macromolecular Assemblies*, Oxford University Press
31 Frank, J. *et al.* (1991) Three-dimensional reconstruction of the 70S *Escherichia coli* ribosome in ice: the distribution of ribosomal RNA. *J. Cell Biol.* 115, 597–605
32 Gabashvili, I.S. *et al.* (2000) Solution structure of the *E. coli* 70S ribosome at 11.5 Å resolution. *Cell* 100, 537–549
33 Kühlbrandt, W. (2014) Biochemistry. The resolution revolution. *Science* 343, 1443–1444
34 Dainty, J.C. and Shaw, R. (1974) *Image Science: Principles, Analysis and Evaluation of Photographic-type Imaging Processes*, Academic Press
35 Hamilton, J.F. and Marchant, J.C. (1967) Image recording in electron microscopy. *J. Opt. Soc. Am.* 57, 232–239
36 McMullan, G. *et al.* (2009) Detective quantum efficiency of electron area detectors in electron microscopy. *Ultramicroscopy* 109, 1126–1143
37 Roberts, P.T.E. *et al.* (1982) A CCD-based image recording system for the CTEM. *Ultramicroscopy* 8, 385–396
38 Spence, J.C.H. and Zuo, J.M. (1988) Large dynamic range, parallel detection system for electron diffraction and imaging. *Rev. Sci. Instrum.* 59, 2102–2105
39 Krivanek, O.L. and Mooney, P.E. (1993) Applications of slow-scan CCD cameras in transmission electron microscopy. *Ultramicroscopy* 49, 95–108
40 Faruqi, A.R. *et al.* (1999) Cooled CCD detector with tapered fibre optics for recording electron diffraction patterns. *Ultramicroscopy* 75, 235–250

41 Suloway, C. *et al.* (2005) Automated molecular microscopy: the new Leginon system. *J. Struct. Biol.* 151, 41–60
42 Sander, B. *et al.* (2005) Advantages of CCD detectors for de novo three-dimensional structure determination in single-particle electron microscopy. *J. Struct. Biol.* 151, 92–105
43 Booth, C.R. *et al.* (2004) A 9 angstroms single particle reconstruction from CCD captured images on a 200 kV electron cryomicroscope. *J. Struct. Biol.* 147, 116–127
44 Faruqi, A.R. and McMullan, G. (2011) Electronic detectors for electron microscopy. *Q. Rev. Biophys.* 44, 357–390
45 Turchetta, R. *et al.* (2001) A monolithic active pixel sensor for charged particle tracking and imaging using standard VLSI CMOS technology. *Nucl. Instrum. Methods Phys. Res. Sect. Accel. Spectrometers Detect. Assoc. Equip.* 458, 677–689
46 Milazzo, A-C. *et al.* (2005) Active pixel sensor array as a detector for electron microscopy. *Ultramicroscopy* 104, 152–159
47 Faruqi, A.R. *et al.* (2005) Direct single electron detection with a CMOS detector for electron microscopy. *Nucl. Instrum. Methods Phys. Res. Sect. Accel. Spectrometers Detect. Assoc. Equip.* 546, 170–175
48 McMullan, G. *et al.* (2009) Experimental observation of the improvement in MTF from backthinning a CMOS direct electron detector. *Ultramicroscopy* 109, 1144–1147
49 Ruskin, R.S. *et al.* (2013) Quantitative characterization of electron detectors for transmission electron microscopy. *J. Struct. Biol.* 184, 385–393
50 McMullan, G. *et al.* (2014) Comparison of optimal performance at 300keV of three direct electron detectors for use in low dose electron microscopy. *Ultramicroscopy* 147C, 156–163
51 Bichsel, H. (1988) Straggling in thin silicon detectors. *Rev. Mod. Phys.* 60, 663–699
52 McMullan, G. *et al.* (2009) Enhanced imaging in low dose electron microscopy using electron counting. *Ultramicroscopy* 109, 1411–1416
53 Li, X. *et al.* (2013) Electron counting and beam-induced motion correction enable near-atomic-resolution single-particle cryo-EM. *Nat. Methods* 10, 584–590
54 Li, X. *et al.* (2013) Influence of electron dose rate on electron counting images recorded with the K2 camera. *J. Struct. Biol.* 184, 251–260
55 Gao, H. *et al.* (2004) Dynamics of EF-G interaction with the ribosome explored by classification of a heterogeneous cryo-EM dataset. *J. Struct. Biol.* 147, 283–290
56 Valle, M. *et al.* (2002) Cryo-EM reveals an active role for aminoacyl-tRNA in the accommodation process. *EMBO J.* 21, 3557–3567
57 Sigworth, F.J. (1998) A maximum-likelihood approach to single-particle image refinement. *J. Struct. Biol.* 122, 328–339
58 Scheres, S.H.W. *et al.* (2007) Disentangling conformational states of macromolecules in 3D-EM through likelihood optimization. *Nat. Methods* 4, 27–29
59 Elad, N. *et al.* (2008) Detection and separation of heterogeneity in molecular complexes by statistical analysis of their two-dimensional projections. *J. Struct. Biol.* 162, 108–120
60 Zhang, W. *et al.* (2008) Heterogeneity of large macromolecular complexes revealed by 3D cryo-EM variance analysis. *Structure* 16, 1770–1776
61 Spahn, C.M. and Penczek, P.A. (2009) Exploring conformational modes of macromolecular assemblies by multiparticle cryo-EM. *Curr. Opin. Struct. Biol.* 19, 623–631
62 Lyumkis, D. *et al.* (2013) Likelihood-based classification of cryo-EM images using FREALIGN. *J. Struct. Biol.* 183, 377–388
63 Scheres, S.H.W. (2012) A Bayesian view on cryo-EM structure determination. *J. Mol. Biol.* 415, 406–418
64 Scheres, S.H.W. (2012) RELION: Implementation of a Bayesian approach to cryo-EM structure determination. *J. Struct. Biol.* 180, 519–530
65 Brilot, A.F. *et al.* (2012) Beam-induced motion of vitrified specimen on holey carbon film. *J. Struct. Biol.* 177, 630–637
66 Campbell, M.G. *et al.* (2012) Movies of ice-embedded particles enhance resolution in electron cryo-microscopy. *Structure* 20, 1823–1828
67 Bai, X-C. *et al.* (2013) Ribosome structures to near-atomic resolution from thirty thousand cryo-EM particles. *Elife* 2, e00461
68 Cao, E. *et al.* (2013) TRPV1 structures in distinct conformations reveal activation mechanisms. *Nature* 504, 113–118
69 Liao, M. *et al.* (2013) Structure of the TRPV1 ion channel determined by electron cryo-microscopy. *Nature* 504, 107–112
70 Allegretti, M. *et al.* (2014) Atomic model of the F420-reducing [NiFe] hydrogenase by electron cryo-microscopy using a direct electron detector. *Elife* 3, e01963
71 Amunts, A. *et al.* (2014) Structure of the yeast mitochondrial large ribosomal subunit. *Science* 343, 1485–1489
72 Emsley, P. *et al.* (2010) Features and development of Coot. *Acta Crystallogr. D: Biol. Crystallogr.* 66, 486–501
73 Murshudov, G.N. *et al.* (1997) Refinement of macromolecular structures by the maximum-likelihood method. *Acta Crystallogr. Sect. D* 53, 240–255
74 DiMaio, F. *et al.* (2013) Cryo-EM model validation using independent map reconstructions. *Protein Sci.* 22, 865–868
75 Falkner, B. and Schröder, G.F. (2013) Cross-validation in cryo-EM-based structural modeling. *Proc. Natl. Acad. Sci. U.S.A.* 110, 8930–8935
76 Wong, W. *et al.* (2014) Cryo-EM structure of the Plasmodium falciparum 80S ribosome bound to the anti-protozoan drug emetine. *Elife* Published online June 9, 2014, http://dx.doi.org/10.7554/eLife.03080
77 Lu, P. *et al.* (2014) Three-dimensional structure of human γ-secretase. *Nature* 512, 166–170
78 Scheres, S.H. (2014) Beam-induced motion correction for sub-megadalton cryo-EM particles. *Elife* 3, e03665
79 Fernández, I.S. *et al.* (2013) Molecular architecture of a eukaryotic translational initiation complex. *Science* 342, 1240585
80 Koh, C.S. *et al.* (2014) Taura syndrome virus IRES initiates translation by binding its tRNA-mRNA-like structural element in the ribosomal decoding center. *Proc. Natl. Acad. Sci. U.S.A.* 111, 9139–9144
81 Fernández, I.S. *et al.* (2014) Initiation of translation by cricket paralysis virus IRES requires its translocation in the ribosome. *Cell* 157, 823–831
82 Stark, H. *et al.* (1996) Electron radiation damage to protein crystals of bacteriorhodopsin at different temperatures. *Ultramicroscopy* 63, 75–79
83 Sader, K. *et al.* (2013) Cryomicroscopy of radiation sensitive specimens on unmodified graphene sheets: reduction of electron-optical effects of charging. *J. Struct. Biol.* 183, 531–536
84 Russo, C.J. and Passmore, L.A. (2014) Controlling protein adsorption on graphene for cryo-EM using low-energy hydrogen plasmas. *Nat. Methods* 11, 649–652
85 Marr, C.R. *et al.* (2014) Fabrication of carbon films with ~500 nm holes for cryo-EM with a direct detector device. *J. Struct. Biol.* 185, 42–47
86 Berriman, J.A. and Rosenthal, P.B. (2012) Paraxial charge compensator for electron cryomicroscopy. *Ultramicroscopy* 116, 106–114
87 Grigorieff, N. (2007) FREALIGN: high-resolution refinement of single particle structures. *J. Struct. Biol.* 157, 117–125
88 Ludtke, S.J. *et al.* (1999) EMAN: semiautomated software for high-resolution single-particle reconstructions. *J. Struct. Biol.* 128, 82–97
89 Liu, X. *et al.* (2007) Averaging tens to hundreds of icosahedral particle images to resolve protein secondary structure elements using a Multi-Path Simulated Annealing optimization algorithm. *J. Struct. Biol.* 160, 11–27
90 Kostyuchenko, V.A. *et al.* (2014) Near-atomic resolution cryo-electron microscopic structure of dengue serotype 4 virus. *J. Virol.* 88, 477–482
91 Veesler, D. *et al.* (2013) Atomic structure of the 75 MDa extremophile Sulfolobus turreted icosahedral virus determined by CryoEM and X-ray crystallography. *Proc. Natl. Acad. Sci. U.S.A.* 110, 5504–5509
92 Van Heel, M. *et al.* (1996) A new generation of the IMAGIC image processing system. *J. Struct. Biol.* 116, 17–24
93 Greber, B.J. *et al.* (2013) Architecture of the large subunit of the mammalian mitochondrial ribosome. *Nature* 505, 515–519